Tensile Cracking Behaviour of Strain-Hardening Cement-Based Composites using a Micromechanical Lattice Model

Andrea Carpinteri, Roberto Brighenti, Andrea Spagnoli, Sabrina Vantadori

Department of Civil-Environmental Engineering and Architecture, University of Parma, Viale Usberti 181/A, 43100 Parma, Italy; Fax: +39 0521 905924; E-mail: spagnoli@unipr.it

ABSTRACT. *The crack paths in strain-hardening cement-based composites under tensile loading are simulated using a two-dimensional lattice model. A regular triangular lattice model (formed by truss elements) accounting for the actual multiphase meso-scale structure of the material is developed. The trusses are assumed to have a linear elastic behavior in compression, whereas in tension a linear elastic behavior up to a first cracking stress is followed by an inelastic post-cracking curve. Some numerical results related to tensile specimens are presented in order to investigate the influence of microstructure characteristics of the material on its ductility.*

INTRODUCTION

Strain-hardening cement-based composites (also called pseudo-ductile cementitious composites or Engineered Cementitious Composites, ECC), a special class of high-performance fiber-reinforced cementitious composites, have been developed to achieve specific composite performances which can be designed on the basis of the micromechanics of the material [1-3]. Under tensile loading, in contrast to normal concrete where a single unstable crack develops, ECC develop multiple stable micro-cracks bridged by fibers. Consequently, tensile stress-strain curves of ECC exhibit a strain-hardening response with a superior ductility (ultimate strain up to 8%, with a certain degree of scattering), which is several hundred times that of normal concrete [4]. The multiple micro-cracking behavior of ECC is strongly dependent on the fiber crack bridging law, in relation to the so-called steady-state (SS) condition for crack propagation [5], and on the degree of heterogeneity in the material, in relation to the condition for crack initiation. Typically, crack initiation sites in ECC material are at material flaws, which are voids (bubbles of entrapped air) in the majority of cases. Consequently, crack initiation behavior is influenced by the size and spatial distribution (both factors are random in nature) of voids in the material [6]. Note that SS cracks are characterized by a flat profile, and the condition for SS cracking is (see [5]):

$$\sigma_0 w_0 - \int_0^{w_0} \sigma(w)\mathrm{d}w \geq G_f \tag{1}$$

where G_f = fracture energy of the matrix, σ_0 = peak stress of the fiber crack bridging law, w_0 = crack opening displacement at the peak stress of the fiber crack bridging law.

Some theoretical models are available in the literature to describe the tensile behaviour of ECC (e.g. see [7,8]). However, the detailed links between material microstructure and composite performance requires further investigations, for instance through micromechanical models such as lattice models [9]. In the present paper, the crack paths in ECC under tensile loading are analysed using a two-dimensional lattice model [10,11]. A regular triangular lattice model (formed by truss elements) accounting for the actual multiphase meso-scale structure of the material is developed. The trusses are assumed to have a linear elastic behavior in compression, whereas in tension a linear elastic behavior up to a first cracking stress is followed by a linear inelastic piecewise post-cracking curve with softening branches. Some numerical results for ECC tensile specimens are presented along with those for a standard Fiber-Reinforced Cementitious Composite (FRCC) in order to investigate the influence of void distribution in the material on its ductility.

THE LATTICE MODEL

A two-dimensional lattice is adopted to discretize the continuum model of the material. Such a lattice is regular triangular (i.e. with hexagonal unit cells), and truss elements are used. The length l of the truss elements dictates the level of the discretization (Fig. 1). The Young modulus of the truss elements in the lattice model determines the stiffness of the continuum discretized through the lattice. The relationship between the Young modulus of the truss ($\overline{E}$) and that of the continuum (E) is given by [12]:

$$\overline{E} = \frac{\sqrt{3}l}{2A} E \tag{2}$$

where A is the cross-sectional area of the truss elements. From now onwards we use the following notation: a bar above the symbol means that the quantity is related to truss elements of the lattice model, whereas the plain symbol means that the quantity is related to the continuum model. The adopted lattice of truss elements enforces a Poisson ratio of the continuum equal to 1/3 [9]. Considering a plane stress field acting in the continuum (with the 3 components $\sigma_x, \sigma_y, \tau_{xy}$ in the xy frame), the following transformation rule for stresses can be derived [10]:

$$\begin{Bmatrix} \overline{\sigma}^{(1)} \\ \overline{\sigma}^{(2)} \\ \overline{\sigma}^{(3)} \end{Bmatrix} = \frac{l}{A} \begin{bmatrix} \sqrt{3}/2 & -\sqrt{3}/6 & 0 \\ 0 & \sqrt{3}/3 & 1/2 \\ 0 & \sqrt{3}/3 & -1/2 \end{bmatrix} \begin{Bmatrix} \sigma_x \\ \sigma_y \\ \tau_{xy} \end{Bmatrix} \tag{3}$$

where $\overline{\sigma}^{(1)}$, $\overline{\sigma}^{(2)}$ and $\overline{\sigma}^{(3)}$ are the axial stresses acting in the trusses.

In the continuum model, the tensile behaviour of a fiber-reinforced cementitious composite can be described according to the cohesive crack approach (e.g. see Ref.

[13,14] also in relation to localization problems which can be encountered in cohesive crack models). Hence, the stress-strain curve is the result of the contribution of three constituting laws: the constitutive law of solid concrete (bulk material), assumed to be linear with Young modulus in tension equal to that in compression; the crack bridging law of plain concrete; the crack bridging law due to fibers. The resulting stress-strain curve is characterized by a perfectly elastic behaviour in compression; the tensile behavior is elastic up to a first cracking stress, and a linear piecewise postcracking curve with softening branches follows.

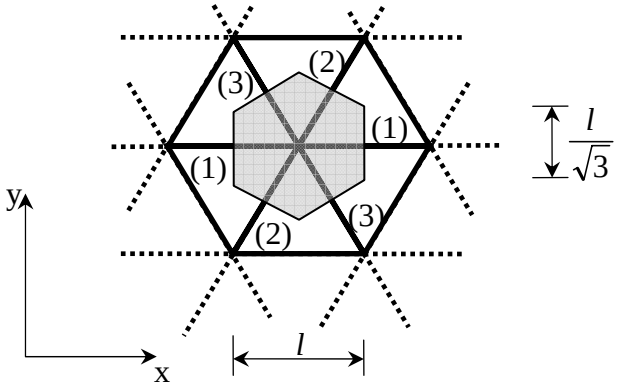

Figure 1. The unit cell of a regular triangular lattice.

With reference to the lattice model, under uniaxial stress condition the stress in the truss parallel to the loading axis is equal to $\bar{\sigma} = \left(l\sqrt{3}/(2A)\right)\sigma$ (e.g. see in Eq. 3 the stress in the truss (1) when *x* is the loading axis). Accordingly, the first cracking stress $\bar{f}_t$ of the truss is assumed to be equal to $\left(l\sqrt{3}/(2A)\right)f_t$, where f_t is the first cracking stress of the continuum. The same rule is applied for the peak stress σ_0 of the crack bridging law due to fibers ($\bar{\sigma}_0 = \left(l\sqrt{3}/(2A)\right)\sigma_0$). The strain $\bar{\varepsilon}_{el}$ of the truss at the elastic limit (strain at the first cracking stress) is equal to $\bar{f}_t/\bar{E}$.

In line with the cohesive crack approach, the area under the stress σ against crack opening w curve (characterized by a first cracking stress f_t and an ultimate crack opening w_u) is equal to the Mode I fracture energy G_f (hence, for a linear curve σ against w, we have $w_u = 2G_f/f_t$). This concept can be translated to the truss elements of the lattice model. Hence, the ultimate cracking strain $\bar{\varepsilon}_u$ is given by:

$$\bar{\varepsilon}_u = 2\frac{\bar{G}_f}{l\bar{f}_t} \tag{4}$$

where $\bar{G}_f$ is the Mode I fracture energy of the truss, and can be determined from the continuum counterpart following an energy conservation argument (that is, the energy dissipation at surface of the crack in the continuum is lumped at the cross-sectional area of the truss). Hence, by considering the influence area (equal to $l/\sqrt{3}$) assigned to a

truss submitted to a pure Mode I loading (e.g. see the truss (1) in Fig. 1, submitted to the uniaxial stress σ_x), we have:

$$\overline{G}_f = \frac{l}{A\sqrt{3}} G_f \tag{5}$$

The characteristic cracking strain values of the crack bridging curve due to fibers can be obtained by smearing the crack opening along the length of the truss, namely:

$$\bar{\varepsilon}_0 = \frac{w_0}{l}, \ \bar{\varepsilon}_{u,f} = \frac{w_{u,f}}{l} \tag{6}$$

where w_0 = crack opening at the peak stress of the crack bridging law due to fibers; $w_{u,f}$ = ultimate crack opening of the bridging law due to fibers. Note that typically $w_{u,f}$ is taken to be equal to a half the fiber length [15]. Finally, the resulting stress-strain curve in the truss elements of the lattice model (see Fig. 2) can be obtained once the following values of stress/strain are computed:

$$\bar{\sigma}_1 = \begin{cases} \bar{\sigma}_0 + \bar{f}_t \dfrac{\bar{\varepsilon}_u - \bar{\varepsilon}_0}{\bar{\varepsilon}_u} & \text{if } \bar{\varepsilon}_0 < \bar{\varepsilon}_u \\ \bar{\sigma}_0 \dfrac{\bar{\varepsilon}_u}{\bar{\varepsilon}_0} & \text{if } \bar{\varepsilon}_0 \geq \bar{\varepsilon}_u \end{cases} \qquad \bar{\varepsilon}_1 = \begin{cases} \dfrac{\bar{\sigma}_1}{\bar{E}} + \bar{\varepsilon}_0 & \text{if } \bar{\varepsilon}_0 < \bar{\varepsilon}_u \\ \dfrac{\bar{\sigma}_1}{\bar{E}} + \bar{\varepsilon}_u & \text{if } \bar{\varepsilon}_0 \geq \bar{\varepsilon}_u \end{cases} \tag{7a}$$

$$\bar{\sigma}_2 = \begin{cases} \bar{\sigma}_0 \dfrac{\bar{\varepsilon}_{u,f} - \bar{\varepsilon}_u}{\bar{\varepsilon}_{u,f} - \bar{\varepsilon}_0} & \text{if } \bar{\varepsilon}_0 < \bar{\varepsilon}_u \\ \bar{\sigma}_0 & \text{if } \bar{\varepsilon}_0 \geq \bar{\varepsilon}_u \end{cases} \qquad \bar{\varepsilon}_2 = \begin{cases} \dfrac{\bar{\sigma}_2}{\bar{E}} + \bar{\varepsilon}_u & \text{if } \bar{\varepsilon}_0 < \bar{\varepsilon}_u \\ \dfrac{\bar{\sigma}_2}{\bar{E}} + \bar{\varepsilon}_0 & \text{if } \bar{\varepsilon}_0 \geq \bar{\varepsilon}_u \end{cases} \tag{7b}$$

where the strains $\bar{\varepsilon}_1$ and $\bar{\varepsilon}_2$ above are the sum of elastic strains ($\bar{\sigma}_1/E$ and $\bar{\sigma}_2/E$) and cracking strains ($\bar{\varepsilon}_0$ and $\bar{\varepsilon}_u$). If, at a certain load step, the tensile strain $\bar{\varepsilon}$ in the truss is higher than $\bar{\varepsilon}_{el}$, an iterative procedure up to convergence is performed using a secant stiffness approach ($\bar{E}^{(i)}$ is the secant Young modulus after convergence at the i-th load step, see Fig. 2).

The modeling of material heterogeneities at the meso-scale level is carried out following an automatic procedure. We consider synthetically-generated microstrutures of the material where the particles of each phase are assumed to be circular. The size distribution of the particles for each phase follows statistics (e.g. with a Gaussian or uniform Probability Density Function, PDF), whereas the spatial distribution of the particles is assumed to be characterized by a uniform PDF. Then, a regular triangular lattice is laid over the synthetic microstructure so that different mechanical properties are attributed to each truss element of the lattice depending on the region (phase) into which the element is located. In the following, the heterogeneity of the examined cementitious composites (which do not contain coarse aggregates) is analysed at the meso-scale level by treating the material as a 2-phase composite with mortar (cement paste or matrix) and voids of entrapped air. Therefore, matrix and void elements are

considered in the lattice model.

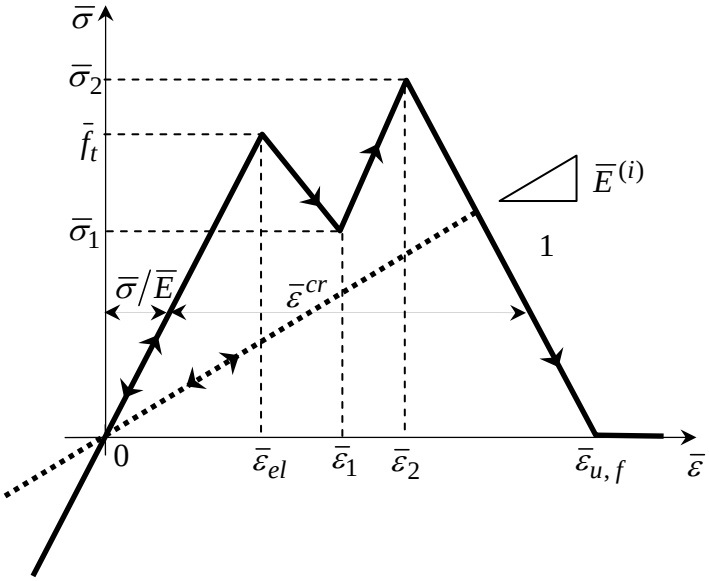

Figure 2. The resulting stress-strain curve (not to scale) in the truss elements of the lattice model ($\bar{E}^{(i)}$ is the secant Young modulus in the cracking stage at the *i*-th load step) in a typical case of ECC (Engineered Cementitious Composite).

SIMULATIONS

A rectangular specimen under tensile load acting in the direction of the major axis is analysed. The tensile load is applied under displacement control along the minor sides of the specimen. The aim of the simulations is to investigate the tensile ductility of ECC with reference to its multicracking features. For comparison, a standard FRCC (for which the condition of SS cracking, see Eq. 1, is not fulfilled) is analysed.

The volume fraction of voids is taken as equal to 7%, and the void diameter range $\Delta D = D_{\max} - D_{\min}$ varies in the interval 1 to 5 mm. A Gaussian PDF for the diameter distribution of voids, such that there is a 95% probability of occurrence in the range ΔD, is adopted.

The input parameters for FRCC and ECC are: E = 20GPa, f_t = 5MPa, G_f = 12J/m^2, w_u = 4.8μm, σ_0 = 6MPa, $w_{u,f}$ = 6mm (the values related to crack-bridging law due to fibers are typical of an ECC containing 2% by volume of polyvinyl alcohol fibers with a length equal to 12mm). The value of the crack opening w_0 is equal to 2 and 20 μm for FRCC and ECC, respectively. This is to ensure the SS crack growth for ECC (as a matter of fact, assuming a linear piecewise fiber crack bridging law σ-w, the inequality of Eq. 1 is fulfilled), but not for FRCC. The material parameters of the truss elements in the lattice model can be obtained using Eqs 2 to 7 for the adopted lattice size l equal to 1mm. A negligible value of stiffness for the void elements is assumed.

In a series of simulations, the maximum diameter of voids is kept constant and their diameter range ΔD is made to vary. Then, a series of simulations where ΔD is kept constant is performed. A summary of the considered diameter range of voids is reported in the table displayed in Fig. 4.

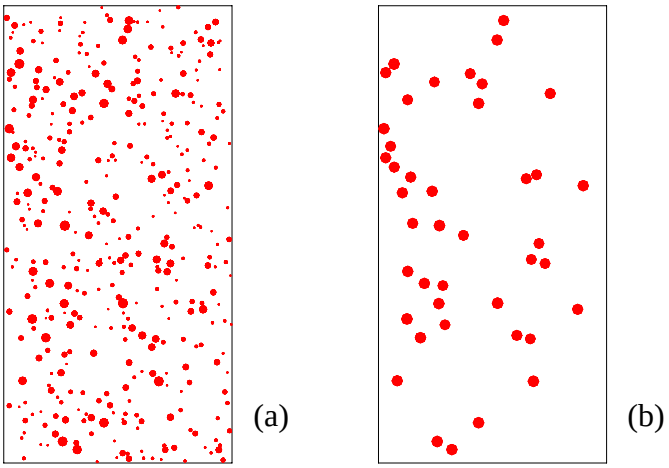

Figure 3. Void distribution for diameter range equal to: (a) 0.5 to 5 mm; (b) 4 to 5 mm.

Figure 4 shows the stress-strain curves for FRCC and ECC with all the void distributions being considered. Firstly, the superior ductility of ECC is clearly demonstrated by the curves. Such a different strain-hardening behaviour of ECC as compared to the softening one of FRCC, well-known from experiments, is hence fairly well described in the simulations by the present lattice model. Then, it can be noted that the peak stress is slightly affected by the void distribution in both FRCC and ECC. On the other hand, the strain at peak stress is marginally affected by the void distribution in FRCC, while the opposite occurs in ECC. In more detail, we can see that strain ductility in ECC tends to increase as the minimum void size increases.

Multiple cracking, which is responsible for the higher ductility of ECC, is also well simulated by the present lattice model. As a matter of fact, Fig. 5 reports, for a sample case, the contour plots in the deformed mesh of the damage variable $1-\overline{E}^{(i)}/\overline{E}$ ($\overline{E}^{(i)}$ is the current secant Young modulus) at increasing overall strain. Red colour is used to indicate the truss elements where the damage variable is equal to unity. Hence, red regions illustrate the crack paths developing in the model: FRCC model shows a single main crack, while the cracking in ECC model is spread along the specimen height.

CONCLUSIONS

The crack paths in cementitious composites under tensile loading are examined using a two-dimensional triangular lattice model, which accounts for the actual multiphase

structure (at the meso-scale level) of the material. Treating fiber-reinforced cementitious composites as 2-phase composites (mortar matrix and air voids), tensile tests are simulated using the above model to analyse their tensile capacity. The tensile strain capacity for a typical ECC is compared to that for a standard FRCC. The adopted lattice model presents the advantage to describe void distribution in the material, which plays a major role in the tensile strain capacity of ECC. The results of the simulations demonstrate that the tensile strain capacity is affected by void distribution only for ECC. In more detail, the simulations show that the tensile strain at the peak stress tends to increase as the minimum size of the void range increases.

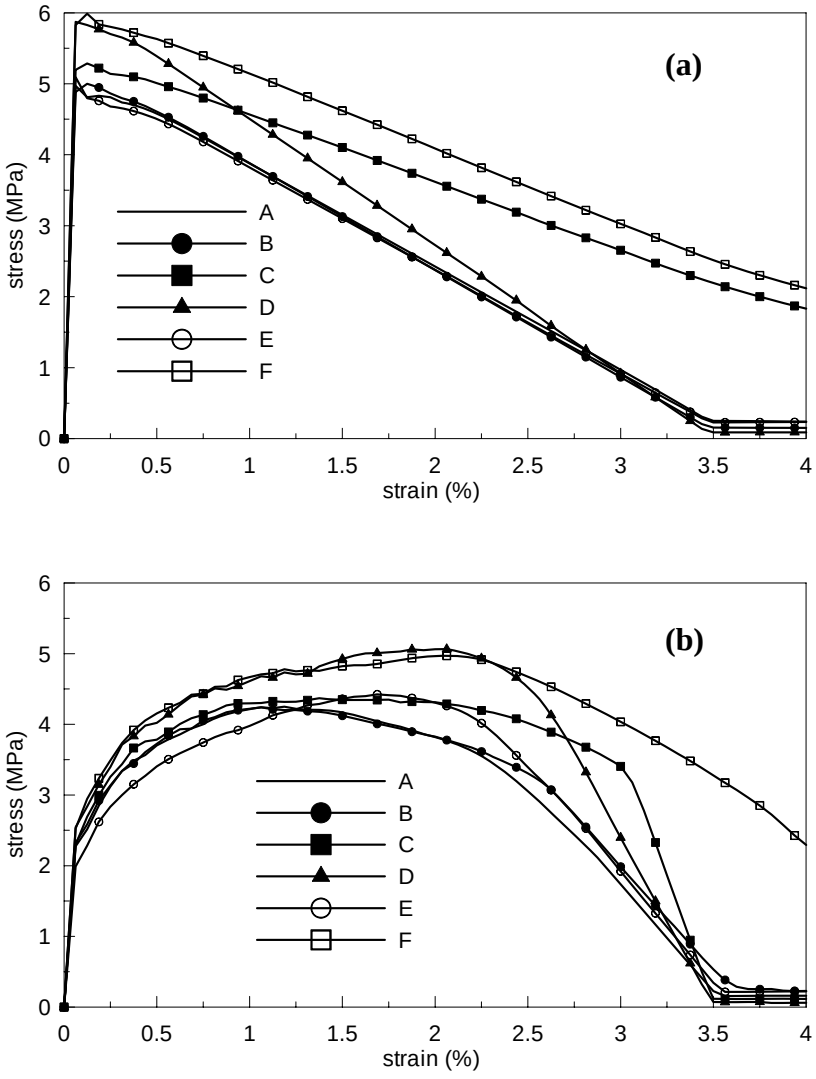

	Void size range (mm)
A	0.5 to 5.0
B	1.0 to 5.0
C	2.0 to 5.0
D	4.0 to 5.0
E	0.5 to 2.5
F	3.0 to 5.0

Figure 4. Comparison of overall σ-ε curves for: (a) FRCC; (b) ECC.

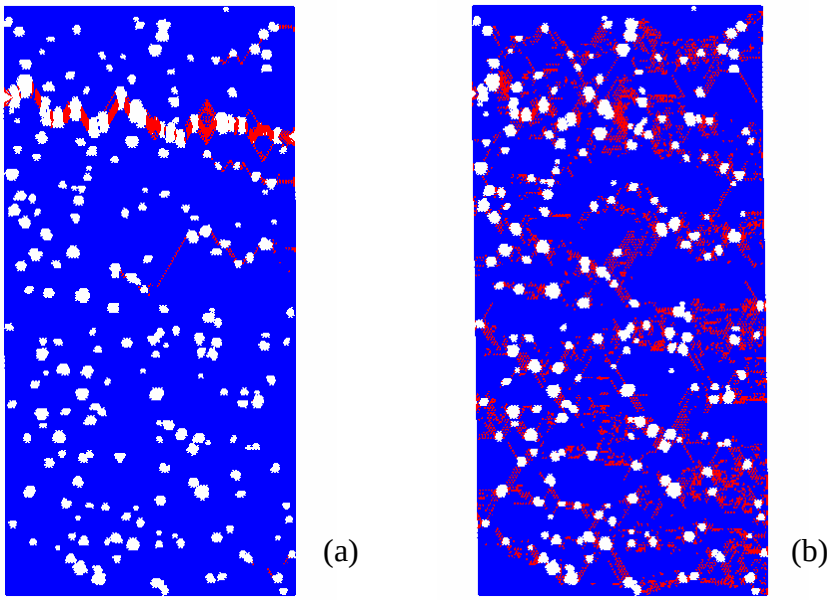

(a) (b)

Figure 5. Contour of the damage variable $1-\overline{E}^{(i)}/\overline{E}$ at overall strain of 1% (red cotour corresponds to a damage equal to unity) in the case of diameter range of voids 1 to 5 mm for : (a) FRCC; (b) ECC.

REFERENCES

1. Li, V.C. (1993) *Structural Eng./Earthquake Eng. JSCE* **10**: 37-48.
2. Leung, C.K.Y., Cheung, A.K.F. and Zhang, X.F. (2006) *Book Series: Key Engineering Materials*, **312**: 319-324.
3. van Zijl, G.P.A.G (2007) *Cement Concrete Res.* **37**: 1241-1247.
4. Li, V.C., Wang, S. and Wu, C. (2001) *ACI Mater. J.* **98**: 483–492.
5. Marshall, D.B. and Cox, B.N. (1988) *Mech. Mater.* **7**: 127–133.
6. Li, V.C. and Wang, S. (2006) *Probabilist. Eng. Mech.* **21**: 201–206.
7. Kabele, P. (2007) *Eng. Fract. Mech.* **74**: 194–209.
8. Spagnoli, A., Yang, E.-H. and Li, V.C. (2008). In: *Proceedings of the 17th Biennial European Conference on Fracture (ECF 17)*, pp. 2407-2414.
9. Schlangen, E. and van Mier, J.G.M. (1992) *Mater. Struct.* **25**: 534-542.
10. Spagnoli, A. (2009) *Comp. Mater. Sci.* (available online; doi:10.1016/j.commatsci.2009.01.021).
11. Guo, L., Carpinteri, A., Roncella, R., Spagnoli, A., Sun, W. and Vantatori, S. (2009) *Comp. Mater. Sci.* **44**, 1098-1106.
12. Ostoja-Starzewski, M. (2002) *Appl. Mech. Rev.* **55**: 38-40.
13. Carpinteri, Al. (1989) *Eng. Fract. Mech.* **32**: 265-278.
14. Carpinteri, Al. (1989) *Int. J. Numer. Meth. Eng.* **28**: 1521-1537.
15. Li, V.C. (1992) *J. Mater. Civil Eng.* **4**: 41-57.